Dalton Transactions RSCPublishing

ARTICLE

$La_{1-x}Ln_xH(O_3PCH_3)_2$ (Ln=Tb, Eu ; 0<x≤1) : An Organic-Inorganic Hybrid with Lanthanide Chains and Tunable Luminescent Properties

Cite this: DOI: 10.1039/x0xx00000x

Received 00th September 2014, Accepted 00th September 2014

DOI: 10.1039/x0xx00000x

www.rsc.org/

B. Mutelet,[a] S. Boudin,[a] O. Perez,[a] J.M. Rueff,[a] C. Labbé,[b] and P.A. Jaffres[c]

The organic / inorganic $La_{1-x}Ln_xH(O_3PCH_3)_2$ (Ln = Eu, Tb) hybrids have been synthesized by hydrothermal synthesis. The crystal structure of $LaH(O_3PCH_3)_2$ consists of chains of edge-sharing LaO_8 polyhedra linked through PO_3C tetrahedra. Photoluminescence of Eu^{3+}, Tb^{3+} and Eu^{3+}/Tb^{3+} co-doped materials have been investigated. The Eu and Tb hybrids show no concentration quenching versus doping rate suggesting energy migration through a percolation model. The Eu hybrids exhibit a red emission while the Tb ones exhibit, with the Tb rate increasing, a blue to green emission under a 378 nm excitation wavelength and a cyan to green emission under a 262 nm excitation wavelength. The doping rate dependent red shift results from cross relaxation phenomenon between closed Tb^{3+} ions. The blue to cyan shift observed for the slightly doped materials, when excitation wavelength shifts from 378 nm to 262 nm, is due to different relaxation phenomenons, from the $^5D_3$ level for a 378 nm excitation wavelength and from the $^5D_4$ level via the 4f5d level for a 262 nm excitation wavelength. Under a 378 nm wavelength, the co-doped $La_{0.93}Eu_{0.03}Tb_{0.04}H(O_3PCH_3)_2$ hybrid exhibits a white/cyan emission with CIE coordinates equal to x = 0.29, y = 0.37.

1 - Introduction

Metal phosphonates have been extensively studied those last decades due to their large potential applications as molecular sieves, ions exchangers, sorbents, catalysts, proton conductors, opto-electronics and non linear optical materials[1-6]. Among those materials, the layered lanthanide aryl and alkyl phosphonates $LnH(O_3PR)_2$ (Ln = Eu, Tb ; R = CH_3, C_2H_5, C_3H_7, C_6H_5) exhibit interesting thermal stability up to 400°C or 500°C and intense luminescence with emission comparable to the Gd_2O_2S:Tb commercial phosphor[7,8]. Luminescence can be also enhanced by nanostructuration as shown for nanorods and dandelion-like particles of $LnH(O_3PC_6H_5)_2$ (Ln = Eu, Tb, Y:Eu, Y:Tb)[9-11]. Despite interesting luminescent properties, the $LnH(O_3PC_nH_{2n+2})_2$ hybrids have been few characterized, particularly their crystal structures have not been detailed due to poor crystallization and systematic formation of twinned crystals. Indeed only the cell parameters and the space group have been reported for the methyl phosphonate $LaH(O_3PCH_3)_2$[12]. In order to understand the influence of the lanthanide ions environment on luminescent properties, we reported herein the crystal structure of $LaH(O_3PCH_3)_2$ and photoluminescence properties of $La_{1-x}Ln_xH(O_3PCH_3)_2$ (Ln = Eu, Tb ; 0<x≤1) doped hybrids.

2 - Experimental

2.1 Synthesis and chemical analyses. The $La_{1-x}Ln_xH(O_3PCH_3)_2$ (x = 0, 0.01, 0.05, 0.1, 0.2, 0.3, 0.5, 0.75, 1 ; Ln=Eu, Tb)) samples have been synthesized under hydrothermal conditions. Methyl phosphonic acid (80mg, 0.83mmol), $La(NO_3)_3.6H_2O$ (1-x×0.415mmol), $Ln(NO_3)_3.5H_2O$ (x×0.415mmol) and urea (37.5mg, 0.63mmol) were dissolved in distilled water (15mL). The resulting solutions were placed in a 23mL PTFE vessel, introduced in a Berghof pressure digestion autoclave and heated from room temperature to 180°C during 6h, at 180°C during 24h and cooled to room temperature in 24h. The obtained mixtures were filtrated, washed with distilled water, rinsed with absolute ethanol, the resulting powder samples were dried in air. %C and %H measured by elemental analyses are in good agreement with the expected values with 7.01%C (calc 7.18%) and 2.55%H (calc 2.11%) for $La_{0.5}Eu_{0.5}H(O_3PCH_3)_2$, 6.53%C (calc 7.05%) and 2.68%H (calc 2.07%) for $EuH(O_3PCH_3)_2$, 6.47%C (calc 7.11%) and 2.57%H (calc 2.09%) for $La_{0.5}Tb_{0.5}H(O_3PCH_3)_2$ and 6.14%C (calc 6.90%) and 2.60%H (calc 2.03%) for $TbH(O_3PCH_3)_2$. ThermoGravimetric Analysis (TGA) of $La_{0.5}Eu_{0.5}H(O_3PCH_3)_2$ have been performed using a TGA 92 Setaram thermogravimetric analyser by heating under O_2 from 25°C to 900°C at 10°/min, by keeping at 900°C for 30 min and by cooling back to 25°C. $La_{0.5}Eu_{0.5}H(O_3PCH_3)_2$ decomposes from 450°C to 800°C with $La_{0.5}Eu_{0.5}PO_4$ and $La_{0.5}Eu_{0.5}P_3O_9$ as resulting products according to X ray diffraction analysis. The total weight loss equal to 6,9 % (calc 6,9%), is in agreement with the reaction : $La_{0.5}Eu_{0.5}H(O_3PCH_3)_2 + 4\ O_2 \rightarrow ½\ La_{0.5}Eu_{0.5}PO_4 + ½\ La_{0.5}Eu_{0.5}P_3O_9 + 2\ CO_2 + 3.5\ H_2O$.

2.2 Powder X-ray diffraction. The powder X-Ray diffraction patterns of $La_{1-x}Ln_xH(O_3PCH_3)_2$ (0≤x≤1); Ln=Eu, Tb) samples were recorded for 5°≤2θ≤90° using a Panalytical X'pert Pro diffractometer with Cu Kα (λ_{av} = 1.5418Å) radiations. No impurity phases were detected.

2.3 Single crystal X-ray diffraction study. From the $LaH(O_3PCH_3)_2$ and $La_{0.5}Tb_{0.5}H(O_3PCH_3)_2$ samples, transparent single crystals were successfully isolated for single crystal X-ray diffraction study. In all the other samples, the crystals were too tiny to perform such studies. A 250 µm x 150 µm x 20 µm single crystal of $LaH(O_3PCH_3)_2$ with a good optical quality was selected from the $LaH(O_3PCH_3)_2$ sample using a stereomicroscope. Preliminary X-ray diffraction investigation was performed at room temperature, using Mo Kα radiations on a Kappa CCD (Bruker Nonius) diffractometer equipped with an Apex2 CCD detector. Large Ω scans were used to control the crystalline quality of different samples and to determine cell parameters. The observation of a systematic lateral splitting of the reflections increasing with Θ reveals the existence of twins. A suitable strategy was calculated to ensure a complete data collection using the Apex2 suite, the cell parameters as well as details of the data collection are reported in supplementary materials[†]. Two sets of reflections corresponding to two twin domains have been indexed and extracted separately. The twin domains are related to a two-fold axis parallel to **c** (pseudo merohedral twin). The intensities of the reflections were then integrated, scaled and corrected from the absorption using the empirical method implemented in TWINABS. A structural model considering the centro symmetric space group $P\bar{1}$ was built up with SUPERFLIP[13] using the charge flipping method. The model was then introduced in the refinement program JANA2006[14], all the atomic positions and the anisotropic displacement parameters (ADP) were refined for all the atoms (except for the H atoms, for which the ADP values have been constrained equal to 1.2 times the ADP values of the adjacent C or O atoms). The twin ratios were refined to 64(5)% and 36(5)% for each domain. Bond valence calculation showing a charge deficit on the O2 and O6 atoms, the hydrogen atoms H1O2 and H1O6 were introduced. The position of the H atoms of the methyl groups and those linked to the oxygen atoms was determined on geometrical considerations. The final Fourrier difference map doesn't show any presence of water molecules. The residual electronic density peaks, located very close to the La atom (at 1,1 Å), cannot correspond to oxygen atoms. Their high density values (up to 4,06 $e^-/ Å^3$) can be explained by difficulties to refine the structural model due to the presence of twins. Atomic parameters and interatomic distances are summarized in Tables 1 and 2. Crystals of $La_{0.5}Tb_{0.5}H(O_3PCH_3)_2$ were selected for single crystals X-ray diffraction. They exhibit twin domains, cell parameters and crystal structure similar to $LaH(O_3PCH_3)_2$ crystals. No La/Tb ordering has been detected.

2.4 Photoluminescence. The $La_{1-x}Ln_xH(O_3PCH_3)_2$ ($0<x\leq1$); Ln = Eu, Tb) PhotoLuminescence Excitation (PLE) and PhotoLuminescence emission (PL) spectra have been measured every 1 nm at Room Temperature (RT) using a Horiba Jobin Yvon Fluorolog-3 spectrofluorimeter having a 450W Xenon lamp. Photoluminescence measurements have been performed on weighted powder, spread over a plate sample holder. Intensities measured from different samples, proportional to the emitting surfaces, were considered proportional to the volumes of samples, themselves considered proportional to the masses of samples (the molar masses of $La_{1-x}Ln_xH(O_3PCH_3)_2$, varying only up to 6% with x and with Ln = Eu, Tb). Consequently, the measured intensities have been normalized for 1 g of sample. The Commission Internationale de l'Eclairage (CIE) coordinates have been calculated using the chromatic functions published by Guild et al[15].

Table 1 : Positional parameters of $LaH(O_3PCH_3)_2$

Atom	x	y	z	u_{iso} (Å)
La1	0.2524(2)	0.26231(13)	0.46194(6)	0.0140(3)
P1	0.8887(4)	0.0622(3)	0.2977(2)	0.0141(6)
P2	-0.3652(4)	0.5750(3)	0.2973(2)	0.0134(6)
O1	0.0763(12)	0.1675(8)	0.2980(7)	0.020(2)
O2	-0.0242(11)	0.1387(8)	0.6747(7)	0.021(2)
O3	0.6732(11)	0.0717(8)	0.4087(7)	0.020(2)
O4	-0.1664(11)	0.4901(8)	0.4098(6)	0.0184(18)
O5	0.4501(12)	0.4679(8)	0.2966(7)	0.021(2)
O6	-0.5062(11)	0.7582(7)	0.3267(6)	0.0173(18)
C1	0.7368(16)	0.1326(13)	0.1370(9)	0.031(3)
C2	-0.2004(15)	0.6156(13)	0.1348(8)	0.028(3)
H1c1	0.8623	0.1017	0.0671	0.037(4)
H2c1	0.6007	0.0755	0.143	0.037(4)
H3c1	0.6652	0.2588	0.1142	0.037(4)
H1c2	-0.0677	0.6719	0.1386	0.033(4)
H2c2	-0.1231	0.5052	0.1116	0.033(4)
H3c2	-0.3213	0.6914	0.0662	0.033(4)
H1o2	-0.0959	0.2449	0.6601	0.025(3)
H1o6	-0.5801	0.8541	0.3421	0.021(3)

Table 2 : Interatomic distances of $LaH(O_3PCH_3)_2$ (Å). Symmetry codes : (i)-x,-y+1,-z+1 ; (ii)-x+1,-y,-z+1 ; (iii) -x+1,-y+1,-z+1 ; (iv) x+1,y,z ; (v) -x,-y,-z+1 ; (vi) x-1,y,z

La1-O1	2.393(8)	P1-O1^{iii}	1.498(8)
La1-O2	2.609(6)	P1-O2^{i}	1.550(6)
La1-O3	2.460(6)	P1-O3	1.526(6)
La1-O3^{i}	2.606(6)	P1-C1	1.776(9)
La1-O4	2.483(5)	P2-O4	1.528(6)
La1-O4^{ii}	2.602(7)	P2-O5^{iv}	1.497(8)
La1-O5	2.406(6)	P2-O6	1.566(6)
La1-O6^{ii}	2.607(7)	P2-C2	1.775(8)
O1-C1^{iv}	2.699(13)	O4-C2	2.696(10)
O2-C1^{i}	2.700(10)	O5-C2^{iii}	2.677(11)
O3-C1	2.660(11)	O6-C2	2.707(11)
O2-H1o2	0.82	C1-H3c1	0.96
O6-H1o6	0.82	C2-H1c2	0.96
C1-H1c1	0.96	C2-H2c2	0.96
C1-H2c1	0.96	C2-H3c2	0.96

3 - Results and discussion

3.1 Structural description of $LaH(O_3PCH_3)_2$. The $LaH(O_3PCH_3)_2$ structure is composed of organic and inorganic layers alternating along **c** (Fig1). The organic layer is composed from a double sheet of protonated methyl phosphonate $H_{0.5}(O_3PCH_3)$ with methyl groups pointing inside the layer and with tetrahedral PO_3C phosphonate groups pointing outside the layer. The inorganic layer is composed from La^{3+} ions ; each La^{3+} ion is surrounded by 8 oxygen atoms from phosphonate groups, forming a LaO_8 polyhedron. This polyhedron is formed by a LaO_5 pentagonal base with one oxygen atom above and two oxygens below. Inside the inorganic layer, the LaO_8 polyhedra are connected by edges and form chains along the (110) direction (Fig 2). The connection of chains is ensured by the PO_3C groups in such a way that each PO_3C tetrahedron shares one edge of one LaO_8 polyhedron of one chain and one corner with one LaO_8 polyhedron of an adjacent chain (Fig 3). Each LaO_8 polyhedron shares two edges with two PO_3C tetrahedra and four corners with four PO_3C tetrahedra. The structure of $LaH(O_3PCH_3)_2$ presents similarities with the $LaH(O_3PC_6H_5)_2$ one. Both structures are built up from organic and inorganic alternating layers. Within both types of inorganic layers : (i) the La^{3+} ions is eight coordinated with oxygen atoms from six PO_3C groups, (ii) the LaO_8 polyhedra share two opposite edges and form chains of LaO_8 polyhedra, (iii) each LaO_8 polyhedron is connected by two edges to two PO_3C groups, and by four corners to four PO_3C groups, (iv) the connection between the LaO_8 chain is ensured by the PO_3C groups, sharing one edge with one LaO_8 polyhedron from one chain and one corner with one LaO_8 polyhedron from an adjacent LaO_8 chain. In $LaH(O_3PC_6H_5)_2$, LaO_8 is a distorted dodecahedron with La-O distances ranging from 2.40(1)Å to 2.67(1)Å, in $LaH(O_3PCH_3)_2$, LaO_8 is a tricapped pentagonal base, with La-O distances ranging from 2.393(8)Å to 2.607(7)Å.

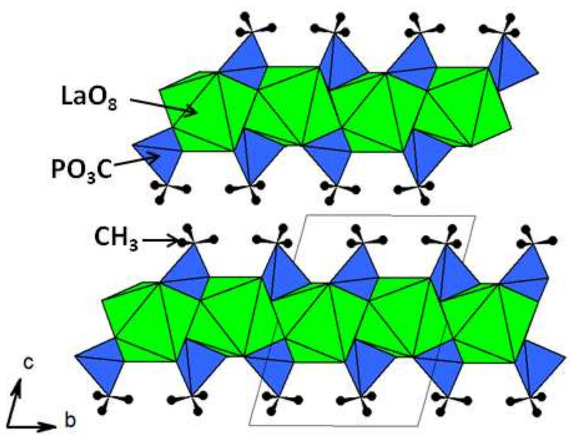

Figure 1. Projection of $LaH(O_3PCH_3)_2$ along a. (The LaO_8 and PO_3C polyhedra are in green and blue, the methyl groups are represented with black balls and sticks)

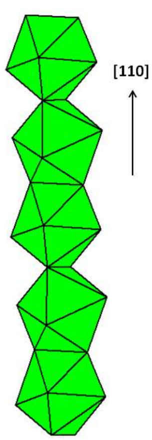

Figure 2. Chain of LaO_8 polyhedra in $LaH(O_3PCH_3)_2$

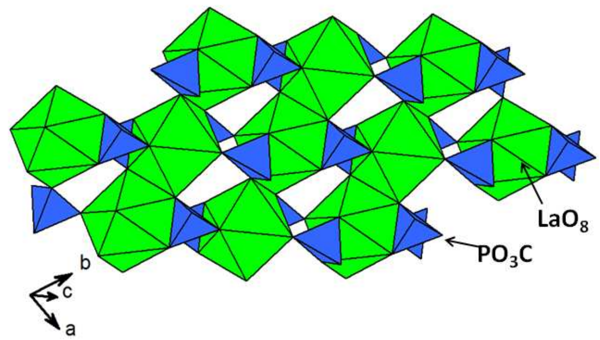

Figure 3. Projection of LaO_8 and PO_3C layer of $LaH(O_3PCH_3)_2$. (The LaO_8 and PO_3C polyhedra are in green and blue)

3.2 Photoluminescence of $La_{1-x}Eu_xH(O_3PCH_3)_2$. The Room Temperature (RT) PhotoLuminescence Excitation (PLE) spectrum of $EuH(O_3PCH_3)_2$ recorded at λ_{em} = 611 nm is plotted on Fig 4. It exhibits bands from 300 to 320 nm, 360 to 390 nm, 390 to 405 nm, at 415nm, at 465 nm, from 525 to 540 nm ascribed to the $^7F_0\rightarrow^5H_6$, $^7F_0\rightarrow^5D_4,^5G_{2-6}$, $^7F_0\rightarrow^5L_6$, $^7F_0\rightarrow^5D_3$, $^7F_0\rightarrow^5D_2$ and $^7F_0\rightarrow^5D_1$ Eu^{3+} transitions respectively[10]. The maximum excitation band is observed for the $^7F_0\rightarrow^5L_6$ transition at 394 nm (Fig 5), it differs from the one reported by Rosa et al.[7] for $EuH(O_3PCH_3)_2$, measured at 378 nm.

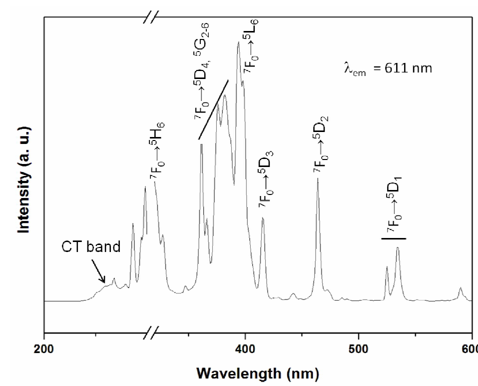

Figure 4. RT PLE spectrum of $EuH(O_3PCH_3)_2$ for λ_{em} = 611 nm

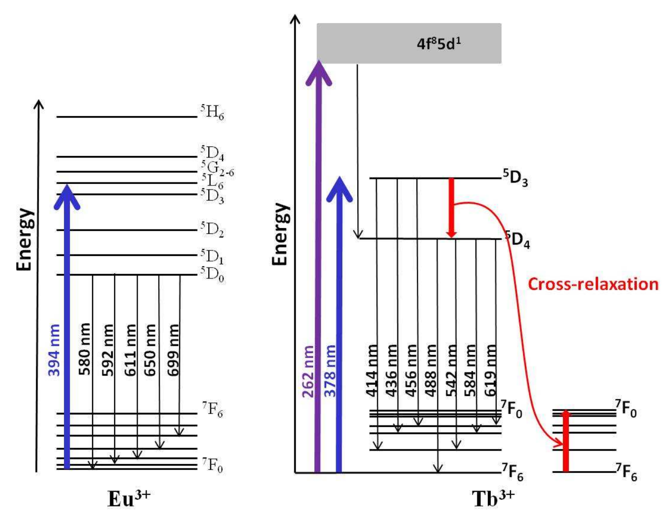

Figure 5. Schema of excitation, relaxation and emission of Eu^{3+} and Tb^{3+} in $La_{1-x}Ln_xH(O_3PCH_3)_2$ (Ln = Eu,Tb)

The RT PhotoLuminescence emission (PL) spectra of $La_{1-x}Eu_xH(O_3PCH_3)_2$ ($0<x\leq1$) recorded for λ_{exc} = 394 nm are plotted on Fig 6. They exhibit bands at 580 nm, from 580 to 603 nm, 603 to 630 nm, 645 to 670 nm, 680 to 710 nm, ascribed to $^5D_0\rightarrow{}^7F_0$, $^5D_0\rightarrow{}^7F_1$, $^5D_0\rightarrow{}^7F_2$, $^5D_0\rightarrow{}^7F_3$ and $^5D_0\rightarrow{}^7F_4$ respectively (Fig 5). The single $^5D_0\rightarrow{}^7F_0$ transition is in agreement with one single crystallographic La^{3+}/Eu^{3+} site, moreover the high intensity ratio $I(^5D_0\rightarrow{}^7F_2)$ / $I(^5D_0\rightarrow{}^7F_1)$ is in agreement with the fact that the Eu^{3+} ions lie on a general 2i position. The emission intensity increases with the Eu^{3+} doping rate as shown on Fig 6 and on Fig 7, where the intensities integrated from 570 to 640 nm are plotted versus the Eu^{3+} doping rate. The maximum emission intensity is clearly observed for $EuH(O_3PCH_3)_2$ from 570 nm to 640nm even though the maximal value of intensity at 611 nm is biased due to detector saturation. No concentration quenching is observed and the maximum of emission occurs for a critical concentration x_c = 1. Such result indicates that concentration quenching in $La_{1-x}Eu_xH(O_3PCH_3)_2$ occurs through a percolation model[16] where x_c verifies the formula $x_c = 2/N$ with N being the number of nearest neighbors Eu^{3+} ions around one Eu^{3+} ion. In $EuH(O_3PCH_3)_2$ where Eu^{3+} ions lie into chains, N is equal to 2 and x_c to 1.

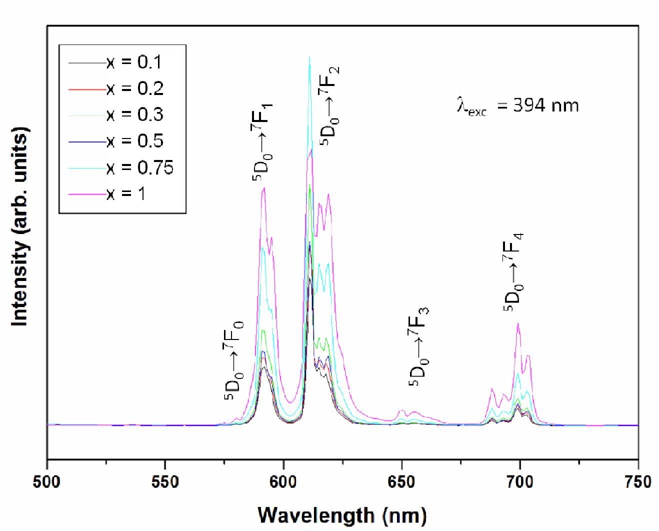

Figure 6. RT PL spectra of $La_{1-x}Eu_xH(O_3PCH_3)_2$ recorded for λ_{exc} = 394 nm

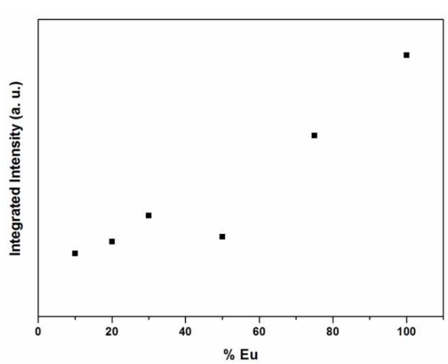

Figure 7. Integrated intensity emitted between 570 nm and 640 nm for $La_{1-x}Eu_xH(O_3PCH_3)_2$ samples under λ_{exc} = 394 nm excitation

3.3 Photoluminescence of $La_{1-x}Tb_xH(O_3PCH_3)_2$. The PLE spectra of $La_{1-x}Tb_xH(O_3PCH_3)_2$ ($0<x\leq1$) recorded for λ_{em} = 543 nm are plotted Fig 8. They exhibit typical 4f-4f excitation bands of Tb^{3+} ions spread from 280 nm to 390 and from 475 nm to 500 nm. The most intense excitation band, centered at 378 nm is assigned to the $^7F_6\rightarrow{}^5D_3$ transition (Fig 5). The spin allowed $4f^8\rightarrow4f^75d$ transition of Tb^{3+}, slightly larger than the 4f-4f transitions, can be observed between 250 nm and 265 nm within a wavelength range usually observed in oxides[17]. The wavelength observed for the maximal intensity shifts slightly from 260 nm to 263 nm when the Tb^{3+} ratio varies from x = 0.01 to 1 as shown in insert on Fig 8. This subtle red shift is in agreement with the nephelauxetic effect expected when the Ln-O bonds become slightly more covalent when Tb^{3+} substitutes La^{3+}. In the present study the $4f^8\rightarrow4f^75d$ transition of Tb^{3+} is rather intense with an excitation intensity equal to 2/3 of the $^7F_6\rightarrow{}^5D_3$ one. The spin forbidden $4f^8\rightarrow4f^75d$ transition of Tb^{3+}, expected at higher wavelength with a weaker emission[17] compared to the spin allowed transition, is hidden by f-f transitions and cannot be observed. All the excitation intensities increase with the Tb^{3+} ratio. Note that the present $TbH(O_3PCH_3)_2$ PLE spectrum differs from the one reported by Rosa et al.[7,8], where the $4f^8\rightarrow4f^75d$ transition is not observed.

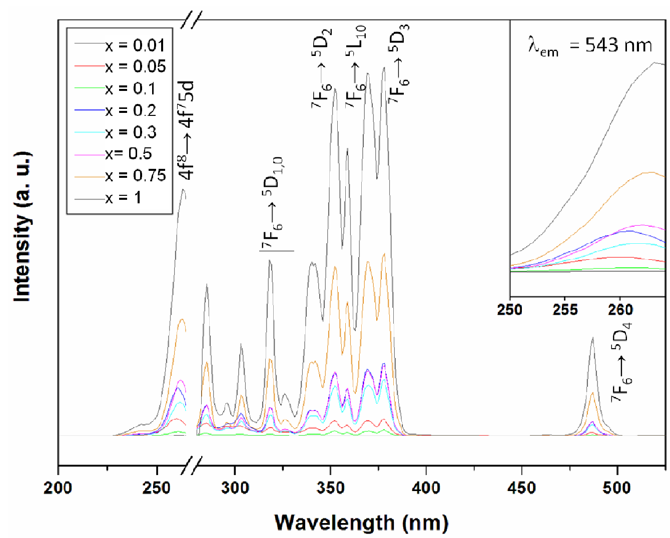

Figure 8. RT PLE spectra of $La_{1-x}Tb_xH(O_3PCH_3)_2$ recorded for λ_{em} = 543 nm ; in insert enlargement of the $4f^8\rightarrow4f^75d$ excitation band.

The PL spectra of $La_{1-x}Tb_xH(O_3PCH_3)_2$ ($0<x\leq1$) recorded at the 4f-4f and 4f→4f5d excitation bands maxima, for λ_{exc} = 378 nm and λ_{exc} = 262 nm respectively, are plotted Fig 9 and 10. Emission bands from 400 nm to 425 nm, from 425 nm to 475 nm, from 475 nm to 510 nm, from 530 nm to 560 nm, from 575 nm to 600 nm and from 615 nm to 630 nm can be assigned to the $^5D_3\rightarrow{}^7F_{5,4}$, $^5D_4\rightarrow{}^7F_{6,5,4,3}$ transitions (Fig 5). The green $^5D_4\rightarrow{}^7F_5$ emission band is the most intense. Under 378 nm and 262 nm excitations, the emission intensities of blue $^5D_4\rightarrow{}^7F_6$, green $^5D_4\rightarrow{}^7F_5$, orange $^5D_4\rightarrow{}^7F_4$ and red $^5D_4\rightarrow{}^7F_3$ transitions increase with the Tb^{3+} rate as shown on the PL spectra (Fig 9 and 10) and on the curves of the integrated intensities of the green $^5D_4\rightarrow{}^7F_5$ transition (Fig 11). Lack of concentration quenching in $La_{1-x}Tb_xH(O_3PCH_3)_2$ suggests energy migration through a percolation model as for Eu^{3+} doped samples. The blue $^5D_3\rightarrow{}^7F_{5,4}$ emission bands, between 400 nm and 475 nm, exhibit different behaviors. Under a 378 nm excitation wavelength, their intensities increase up to a Tb^{3+} rate of x = 0.5 and decrease for higher Tb^{3+} concentration as shown in

insert in Fig 9. This feature can be explained by a cross relaxation phenomenon[18], in which the green emission from the $^5D_4$ level is favor to the detriment of the blue $^5D_3$ emission when the Tb^{3+} concentration increases (Fig 5). Such a phenomenon results from joint $^5D_3 \rightarrow {}^5D_4$ and $^7F_6 \rightarrow {}^7F_0$ transitions between two closed Tb^{3+} ions. Under a 262 nm excitation wavelength, the blue $^5D_3 \rightarrow {}^7F_{5,4}$ emission bands vanish, such phenomenon can be explained by direct relaxation from the 4f5d level to the $^5D_4$ level of Tb^{3+} ions and emissions from this latter level to the $^7F_{6,5,4,3}$ ones (Fig 5). Similar coupled 4f5d / $^5D_4 \rightarrow {}^7F_{6,5,4,3}$ relaxation / emissions have already been observed in phosphors like $Y_3Ga_5O_{12}$:Tb[19]. Under a 378 nm excitation wavelength, relaxation from the $^5D_3$ levels and from the $^5D_4$ levels generate emissions bands from 400 nm to 630 nm.

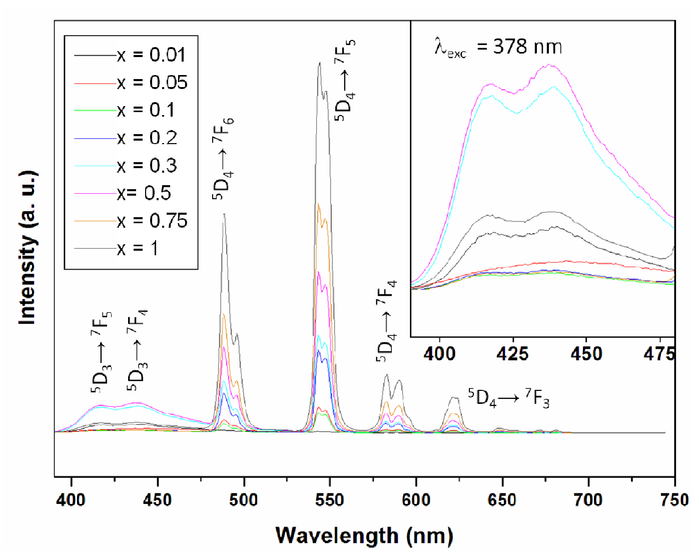

Figure 9. RT PL spectra of $La_{1-x}Tb_xH(O_3PCH_3)_2$ recorded for λ_{exc} = 378 nm ; in insert enlargement of the $5D_3 \rightarrow 7F_{5,4}$ emission band

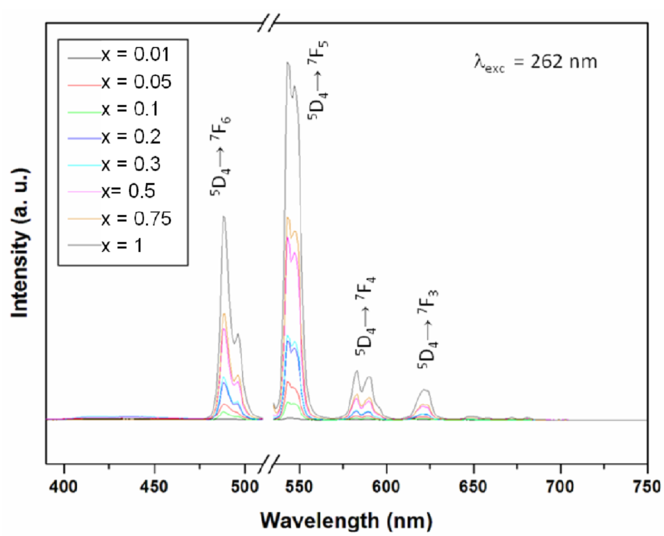

Figure 10. RT PL spectra of $La_{1-x}Tb_xH(O_3PCH_3)_2$ recorded for λ_{exc} = 262 nm

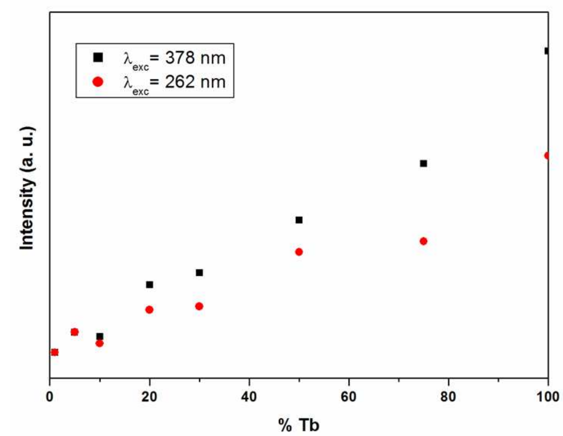

Figure 11. RT Emission intensity of $La_{1-x}Tb_xH(O_3PCH_3)_2$ integrated between 536 nm and 560 nm under 378 nm and 262 nm excitation wavelengths versus Tb^{3+} rate.

The PL spectra of $La_{1-x}Tb_xH(O_3PCH_3)_2$ clearly indicate that emission can be tuned from blue to green either by increasing the Tb^{3+} concentration via cross relaxation phenomenon or by turning the excitation wavelength from near UV (at 378 nm) to UV (at 262 nm). The Figure 12 shows the shifts of the CIE coordinates from blue (x = 0.16 , y = 0.08) to green (x = 0.29 , y = 0.53) as the Tb^{3+} doping rates vary from x = 0.01 to 1 under a 378 nm excitation wavelength and from blue (x = 0.16 , y = 0.08) to cyan (x = 0.24 , y = 0.30) as the x =0.01 doped sample is lighted by near UV (378 nm) or UV (262 nm) radiations.

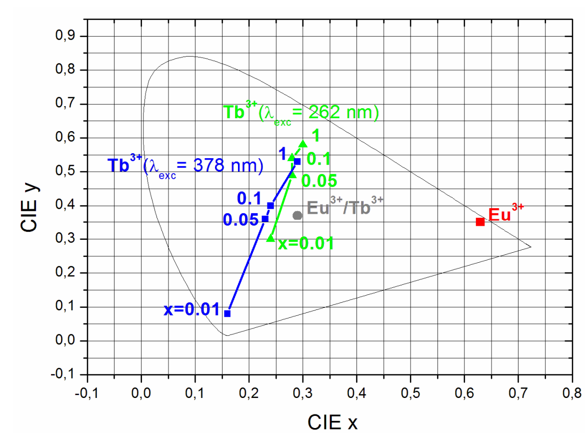

Figure 12. CIE coordinates of $La_{1-x}Ln_xH(O_3PCH_3)_2$ (Ln = Tb ; x = 0.01, 0.05, 0.1, 1 ; λ_{exc} = 262 nm and 378 nm : green and blue curves), (Ln = Eu ; 0<x≤1 ; λ_{exc} = 378 nm : red square) and (Ln_x = $Eu_{0.03}Tb_{0.04}$; λ_{exc} = 378 nm : grey circle)

Conclusion

The organic / inorganic $La_{1-x}Ln_xH(O_3PCH_3)_2$ (Ln = Eu, Tb) hybrids have been synthesized by hydrothermal synthesis. The crystal structure of $LaH(O_3PCH_3)_2$ consists of chains of edge-sharing LaO_8 polyhedra linked through PO_3C tetrahedra. The absence of concentration quenching in the Eu or Tb doped materials can be interpreted by energy migration through a percolation model. The photoemission of the Tb doped material can be adjusted by both the Tb rate and the excitation wavelength, from blue to cyan to green when the Tb rate increases and from blue to cyan when the slightly Tb doped hybrid is exposed to near UV or UV. Since the red Eu and the blue/green Tb hybrids exhibit both large excitation bands at 378 nm, Eu/Tb co-doping has been investigated to synthesize a white phosphor. The slightly doped $La_{0.93}Eu_{0.03}Tb_{0.04}H(O_3PCH_3)_2$ material shows, under a 378 nm wavelength, a white/cyan emission with CIE coordinates (x= 0.29 ; y = 0.37) close to the white (x= 0.33 ; y = 0.33) emission (Fig 12). It is thus an interesting candidate for white phosphor on UV emitting diode. Moreover a $EuH(O_3PCH_3)_2$ / $TbH(O_3PCH_3)_2$ mixture of fully substituted hybrids, deposited on a blue emitting InGaN diode, could be very interesting to generate a device with intense white emission. Compared to other white emitting organic / inorganic hybrids like [La(1,3,5-benzenetricarboxylate)].$(H_2O)_6$: Eu, Tb [20], [Ln(benzimidazole-5,6-dicarboxylate)$_4$(1,10-phenanthroline)$_2(NO_3)$].$2H_2O$ (Ln=Gd,Eu,Tb)[21] or [Zn_3(1,3,5-tri(4-carboxyphenoxy)benzene)$_2(H_2O)_2$].$2H_2O$.4DMF : Tb, Eu[22], $La_{1-x}Ln_xH(O_3PCH_3)_2$ hybrids offer several advantages in one material. Indeed (i) because they are water free, they are highly stable (up to 450°C), (ii) made from the very cheap organic precursor methylphosphonic acid, they can be used for low costs devices and (iii) they can be heavily doped to produce intense emission.

Acknowledgements

The authors acknowledge the financial support of the french Agence Nationale de la Recherche (ANR), through the program "Investissements d'Avenir"(ANR-10-LABX-09-01), Labex EMC[3].

Notes and references

[a] Laboratoire CRISMAT, CNRS UMR6508, ENSICAEN, Université de Caen – Basse Normandie, 6 Bd Maréchal Juin, 14050 Caen Cedex, France

[b] Laboratoire CIMAP, CEA/CNRS UMR6252, ENSICAEN, Université de Caen – Basse Normandie, 6 Bd Maréchal Juin, 14050 Caen Cedex, FRANCE

[c] Université Européenne de Bretagne, Université de Brest, CNRS UMR6521, CEMCA, Av. Victor Le Gorgeu, 29238 Brest, FRANCE

† Space group, cell parameters and agreement factors for $LaH(O_3PCH_3)_2$: $P\bar{1}$ (n°2) ; a=5.3801(10)Å ; b=8.1410(15)Å ; c=10.1367(19)Å ; α=73.807(8)°; β=83.716(8)°; γ=73.693(7)° ; V=408.98(13) Å^3. ; R=0.0473 ; R_w=0.0591.

Electronic Supplementary Information (ESI) available: [S1 : TGA curve of $La_{0.5}Eu_{0.5}H(O_3PCH_3)_2$, X ray diffraction powder patterns of $LaH(O_3PCH_3)_2$, $EuH(O_3PCH_3)_2$ and $TbH(O_3PCH_3)_2$. S2 : CIF of $LaH(O_3PCH_3)_2$]. See DOI: 10.1039/b000000x/

1 Cao, G.; Hong, H.G.; Mallouk, T.E. *Acc. Chem. Res.* **1992**, *25*, 420-427.
2 Thompson, M.E. *Chem. Mater.***1994**, *6*, 1168-1175.
3 Katz, H.E. *Chem. Mater.* **1994**, *6*, 2227-2232.
4 Clearfield, A. *Curr. Opin. Solid State Mat. Sci.* **1996**, *1*, 268-278.
5 Clerafield, A. *Prog. Inorg. Chem.***1998**, *47*, 371.
6 Mao, J.G. *Coord. Chem. Rev.*, **2007**, *251*, 1493-1520.
7 Rosa, I.L.V. ; Nassar, E.J. ; Serra, O.A. *J. Alloys Comp.* **1998**, *275-277*, 315-317.
8 Rosa, I.L.V. ; Santos de Lourenço, A.V. ; Neri, C.R. ; Serra, O.A. *J. Fluoresc.* **2006**, *16*, 455-459.
9 Song, S.Y. ; Ma, J.F. ; Yang, J. ; Cao, M.H. ; Zhang, H.J. ; Wang, H.S. ; Yang, K.Y. *Inorg. Chem.* **2006**, *45*, 1201-1207.
10 Di, W. ; Ferreira, R.A.S. ; Willinger, M.G. ; Ren, X. ; Pinna, *N. J. Phys. Chem. C* **2010**, *114*, 6290-6297.
11 Di, W. ; Ren, X. ; Shirahata, N. ; Liu, C. ; Zhang, L. ; Sakka, Y. ; Pinna, N. *CrystEngComm* **2011,** *13*, 5226-5233.
12 Cao, G. ; Lynch, V.M. ; Swinnea, J.S. ; Mallouk, T.E. *Inorg. Chem.* **1990**, *29*, 2112-2117.
13 Palatinus, L. ; Chapuis, G *J. Appl. Crystallogr.* **2007**, *40*, 786-790.
14 Petricek, V. ; Dusek, M. ; Palatinus, L. *Jana2006. Structure Determination Software Programs* ; Institute of Physics, Praha, Czech Republic, **2006.**
15 Guild, J. *Philosophical Transactions of the Royal Society of London* **1931**, *A230*, 149-187.
16 Berdowski, P.A.M. ; Blasse, G. *J. Solid State Chem.* **1986**, *63*, 86-88.
17 Dorenbos, P. *J. Lumin.* **2000**, *91*, 91-106.
18 Hao, Z. ; Zhang, J. ; Zhang, X. ; Lu, S. ; Wang, X. *J. Electrochem. Soc.* **2009**, *156(3)*, H193-196.
19 Zhu, N. ; Li, Y. ; Yu, X and Ge, W., *J. Lumin.* **2007**, *122-123*, 704-706.
20 Liu, K. ; You, H ; Zheng, Y ; Jia, G. ; Huang, Y. ; Yang, M. ; Song, Y. ; Zhang, L. ; Zhang, H., *Cryst. Growth Des.* **2010**, *10*, 16-19.
21 Ma, X. ; Li, X. ; Cha, Y.E. ; Jin, L.P., *Cryst. Growth Des.* **2012**, *12*, 5227-5232.
22 He, H. ; Sun, F. ; Borjigin, T. ; Zhao, N., Zhu, G. ; *Dalton Trans.*, **2014**, *43*, 3716-3721.

Table of contents

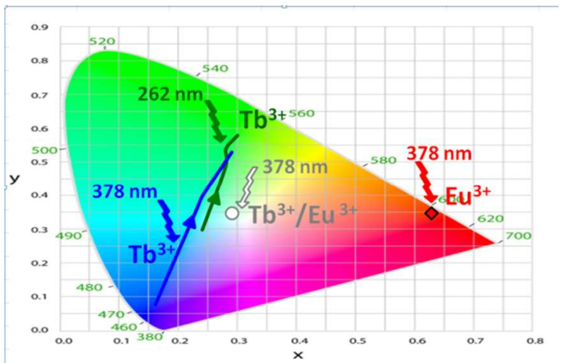

$La_{1-x}Ln_xH(O_3PCH_3)_2$ ($0<x\leq1$); Ln = Eu, Tb) a red, blue to green, cyan to green or white phosphor.